

# Magnetic Sail-Based Displaced Non-Keplerian Orbits

Marco Bassetto\*, Alessandro A. Quarta, Giovanni Mengali

*Dipartimento di Ingegneria Civile e Industriale, University of Pisa, Italy*

---

## Abstract

This paper deals with the problem of determining the requirements for the maintenance of circular, displaced, non-Keplerian orbits around the Sun by means of a magnetic sail-based spacecraft. The magnetic sail is an exotic propellantless propulsion system that gains thrust from the magnetostatic interaction between the solar wind and an artificial magnetic field, which is generated on board by an electrical current flowing through a loop of conducting material. The propulsive requirements are given in terms of characteristic acceleration and thrust (cone) angle. The analysis is performed using a recent mathematical model in which the magnetic sail thrust vector is expressed as a function of the Sun-spacecraft distance and the sail attitude. Moreover, a linear stability analysis is carried out to identify the (marginally) stable displaced orbits when an error in the orbital insertion is assumed.

*Keywords:* magnetic sail, displaced non-Keplerian orbits, mission analysis

---

## Nomenclature

$\mathbf{a}$	=	propulsive acceleration vector (with $a \triangleq \ \mathbf{a}\ $ ), [mm/s <sup>2</sup> ]
$a_c$	=	characteristic acceleration, [mm/s <sup>2</sup> ]
$a_{ij}$	=	coefficients of the linearized dynamics, see Eqs. (39)–(42)
$\{b, c\}$	=	coefficients of the characteristic equation, see Eqs. (45)–(46)
$\{C_D, C_L\}$	=	dimensionless function, see Eqs. (4)–(5)
$d$	=	Earth-spacecraft distance, [au]
$f$	=	auxiliary function; see Eq. (34)
$\{h_0, h_1, k_0, k_1\}$	=	best fit coefficients
$\hat{\mathbf{i}}_r$	=	radial unit vector
$\hat{\mathbf{i}}_\nu$	=	transverse unit vector
$\{\hat{\mathbf{i}}_\rho, \hat{\mathbf{i}}_\theta, \hat{\mathbf{i}}_z\}$	=	unit vectors of $\mathcal{T}_C(\rho, \theta, z)$
$\hat{\mathbf{m}}$	=	dipole moment unit vector
$O$	=	Sun's center of mass
$O'$	=	displaced orbit center
$\mathbf{r}$	=	Sun-spacecraft position vector (with $r \triangleq \ \mathbf{r}\ $ ), [au]
$r_\oplus$	=	reference distance, [au]
$R_{\text{SOI}}$	=	radius of the sphere of influence, [au]
$s$	=	complex variable [1/s]
$S$	=	spacecraft center of mass
$t$	=	time, [years]
$\mathcal{T}_\odot(O; x, y, z)$	=	heliocentric-ecliptic reference frame

---

\*Corresponding author

*Email addresses:* marco.bassetto@ing.unipi.it (Marco Bassetto), a.quarta@ing.unipi.it (Alessandro A. Quarta), g.mengali@ing.unipi.it (Giovanni Mengali)

$\mathcal{T}_C(O; \rho, \theta, z)$	=	rotating cylindrical reference frame
$\alpha$	=	thrust cone angle, [rad]
$\delta_\rho$	=	error in the orbit radius
$\delta_z$	=	error in the orbit displacement
$\eta$	=	thrust coefficient
$\theta$	=	spacecraft azimuthal angle, [rad]
$\lambda$	=	real number
$\mu_\odot$	=	Sun's gravitational parameter, [ $\text{km}^3/\text{s}^2$ ]
$\rho$	=	orbit radius, [m]
$\tau$	=	switching parameter
$\phi$	=	angle of attack, [rad]
$\psi$	=	elevation angle, [rad]
$\omega$	=	angular velocity, [rad/s]
$\bar{\omega}$	=	reference angular velocity (with $\bar{\omega} \triangleq \sqrt{\mu_\odot/r^3}$ ), [rad/s]

### Subscripts

max	=	maximum
0	=	nominal, initial
$\oplus$	=	referred to Earth

### Superscripts

$\wedge$	=	unit vector
$\star$	=	required
$\sim$	=	dimensionless
$'$	=	derivative with respect to $\tilde{t}$
$\cdot$	=	time derivative

## 1. Introduction

The development of continuous-thrust and propellantless propulsion systems has allowed new mission scenarios to be investigated [1, 2, 3, 4, 5]. Among them, closed displaced non-Keplerian orbits (DNKOs) represent a promising option for many applications, as discussed in the survey paper by McKay et al. [6]. The concept of DNKOs has much attracted the scientific interest in the last two decades. For example, Ceriotti et al. [7, 8] analyzed the pole-sitter mission concept, whose aim is to place a spacecraft above one of the Earth's poles for observation purposes. MacDonald et al. [9] discussed a novel concept for an Earth-Mars interplanetary communication relay and a solar storm warning mission by means of high-specific-impulse low-thrust propulsion systems, while Heiligers et al. [10, 11] proposed to design new geostationary orbits by means of a hybrid propulsion system, which combines a solar sail with a solar electric thruster.

Although a DNKO can be approximated with a sequence of Keplerian arcs connected through impulsive maneuvers [12, 13], DNKOs usually require a continuous thrust to be maintained, since their motion plane does not contain the center of mass of the primary body [14]. However, the use of a reaction mass for orbit maintenance limits the mission length and so its scientific return. The use of propellantless propulsion systems, such as solar sails [15], electric solar wind sails [16, 17, 18], or magnetic sails [19, 20, 21, 22, 23], is therefore an attractive choice due to the opportunity they offer to obtain long-lived missions. In this context, McInnes and Bookless [15, 24] suggested the use of solar sail propulsion to generate families of displaced periodic orbits at planetary bodies, Gong et al. [25, 26] investigated the possibility of maintaining elliptic DNKOs by means of solar sails for planetary polar observation and studied the relative orbit design and control methods for formation flying around displaced solar orbits, while Song et al. [27] analyzed solar sail displaced orbits in the Hill's restricted three-body problem. The stability and control of DNKOs generated by low-thrust propulsion systems is studied in Refs. [28, 29]. The relative motion of two spacecraft that track highly non-Keplerian orbits has been discussed by Wang et al. [30]. More recently, Niccolai et al. [31, 32] dealt with both circular and elliptic DNKOs maintained by an electric solar wind sail-based spacecraft.

The aim of this paper is to investigate the problem of generating circular DNKOs by means of a magnetic sail (Magsail), a propellantless propulsion system that was first suggested by Andrews and Zubrin [19, 20,

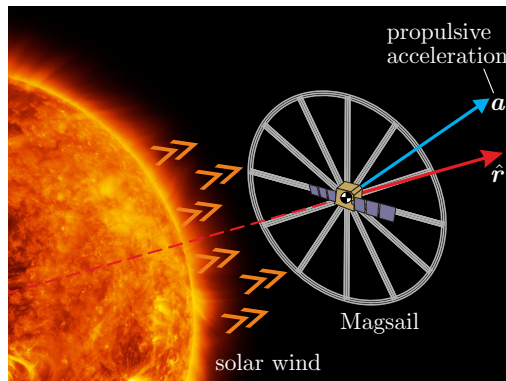


Figure 1: Magsail conceptual scheme.

21, 22, 23]. A Magsail-based spacecraft is essentially constituted by a large coil of superconducting material carrying an electrical current, which generates an artificial magnetic field. The payload is placed at the center of the coil and is connected to it by some support tethers, as is schematically illustrated in Fig. 1. The interaction of ions from the solar wind with the artificial magnetosphere induces a momentum exchange and generates a thrust that is nearly aligned along the Sun-spacecraft direction. Moreover, a transverse thrust component of modest magnitude can be obtained by inclining the plane of the coil. In the last few years, a number of experiments and simulations [33, 34, 35, 36, 37, 38, 39, 40, 41, 42] have given important information about the Magsail performance, and Quarta et al. [43] collected those results to obtain a mathematical model of the Magsail thrust vector suitable for a preliminary mission analysis and design. Such a model is used in this paper for the study of circular DNKO around the Sun and for analyzing their linear stability.

The paper is organized as follows. Section 2 summarizes the mathematical model presented in Ref. [43], section 3 deals with the requirements to be met, in terms of characteristic acceleration and thrust cone angle, for the maintenance of DNKO. Section 4 addresses the problem of analyzing the linear stability regions and, finally, some concluding remarks are given in the last section.

## 2. Thrust vector model

This section summarizes and extends the mathematical thrust model discussed by Quarta et al. [43], who collected the available numerical and experimental data from Refs. [39, 40] to determine an analytical correlation between the sail attitude and the thrust vector characteristics. The simulations and tests described in Refs. [39, 40], together with the pioneering theoretical investigations by Zubrin and Andrews [22], have highlighted that the Magsail thrust vector depends on the heliocentric distance  $r$  and the orientation of the magnetic dipole moment (whose unit vector is  $\hat{\mathbf{m}}$ ) with respect to the Sun-spacecraft unit vector  $\hat{\mathbf{i}}_r$ .

Consider a spacecraft  $S$ , propelled by a Magsail, which moves in the interplanetary space. With reference to Fig. 2, assume  $\hat{\mathbf{i}}_r \times \hat{\mathbf{m}} \neq 0$  and introduce a transverse unit vector

$$\hat{\mathbf{i}}_\nu \triangleq \frac{\hat{\mathbf{i}}_r \times \hat{\mathbf{m}}}{\sin \phi} \times \hat{\mathbf{i}}_r \equiv \frac{\hat{\mathbf{m}} - (\hat{\mathbf{i}}_r \cdot \hat{\mathbf{m}}) \hat{\mathbf{i}}_r}{\sin \phi} \quad (1)$$

where  $\phi \in [-\pi/2, \pi/2]$  rad is the angle of attack, defined as

$$\phi \triangleq \arcsin \left\| \hat{\mathbf{i}}_r \times \hat{\mathbf{m}} \right\| \quad (2)$$

According to Ref. [43], in the general case in which  $\phi \neq 0$ , the propulsive acceleration vector can be written as

$$\mathbf{a} = \tau a_c \left( \frac{r_\oplus}{r} \right)^\eta \left( C_D \hat{\mathbf{i}}_r + C_L \hat{\mathbf{i}}_\nu \right) \quad \text{when} \quad \hat{\mathbf{i}}_r \times \hat{\mathbf{m}} \neq 0 \quad (3)$$

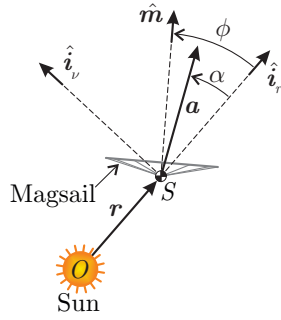


Figure 2: Magsail cone and attack angle.

where  $\tau \in \{0, 1\}$  is a switching parameter, which models the Magsail on/off mode,  $a_c$  is the spacecraft characteristic acceleration, that is, its maximum propulsive acceleration at a Sun-spacecraft distance  $r = r_\oplus \triangleq 1$  au, while  $\eta \in \{4/3, 2\}$  is a dimensionless thrust coefficient that depends on the Magsail size. Two operation modes (either “thin” or “thick”) are usually distinguished in the literature [41], depending on the Magsail size. More precisely, in the “thin” magnetopause mode, which describes the behaviour of a large Magsail with a loop radius on the order of  $10^5$  m, the thrust coefficient is  $\eta = 2$ , while in the “thick” magnetopause mode, consistent with a smaller Magsail and a loop radius on the order of  $10^3$  m, the thrust coefficient is  $\eta = 4/3$  [33, 39]. In Eq. (3),  $C_D = C_D(\phi)$  and  $C_L = C_L(\phi)$  are two dimensionless functions of the angle of attack  $\phi$ , which are obtained in Ref. [43] by interpolating the numerical and experimental data presented in Ref. [41]. The functions  $C_D$  and  $C_L$  are given by

$$C_D = h_0 + h_1 \cos(2\phi) \quad (4)$$

$$C_L = k_0 \sin(2\phi) + k_1 \sin(4\phi) \quad (5)$$

where the (dimensionless) interpolation coefficients  $\{h_0, h_1, k_0, k_1\}$  are reported in Tab. 1 for the two possible Magsail magnetopause modes. Note that, in accordance with the results of Ref. [40],  $C_D$  (or  $C_L$ ) is an even (or odd) function of  $\phi$ . In particular, the function  $C_D$  is always positive, that is,  $\mathbf{a} \cdot \hat{\mathbf{i}}_r \geq 0$ . That means that, similar to what happens for a solar sail [15] or an electric solar wind sail [44], the Magsail can only generate an outward radial thrust component. In the special case in which  $\hat{\mathbf{m}} \equiv \hat{\mathbf{i}}_r$ , that is, when  $\phi = 0$  (see

magnetopause mode	$h_0$	$h_1$	$k_0$	$k_1$	$\eta$
“thin”	0.8133	0.1867	0.1485	0	2
“thick”	0.8312	-0.1688	-0.1338	-0.03969	4/3

Table 1: Best fit coefficients and thrust coefficient  $\eta$  for the two magnetopause modes; see Eqs. (4)-(5).

Fig. 2), Eqs.(4)-(5) give  $C_D = (h_0 + h_1)$  and  $C_L = 0$  and the propulsive acceleration of Eq. (3) reduces to

$$\mathbf{a} = \tau a_c (h_0 + h_1) \left(\frac{r_\oplus}{r}\right)^\eta \hat{\mathbf{i}}_r \quad \text{when} \quad \hat{\mathbf{i}}_r \times \hat{\mathbf{m}} = 0 \quad (6)$$

that is, the Magsail gives a purely outward radial thrust.

Finally, the magnitude of the propulsive acceleration vector is

$$a \triangleq \|\mathbf{a}\| = a_c \left(\frac{r_\oplus}{r}\right)^\eta \sqrt{C_D^2 + C_L^2} \quad (7)$$

while the thrust cone angle  $\alpha$ , that is, the angle between  $\mathbf{a}$  and  $\hat{\mathbf{i}}_r$ , is

$$\alpha = \arctan\left(\frac{C_L}{C_D}\right) \quad (8)$$

The maximum value of the thrust cone angle, referred to as  $\alpha_{\max}$ , depends on the selected magnetopause mode. In particular, for the “thin” mode  $\alpha_{\max} \simeq 10.63$  deg, while  $\alpha_{\max} \simeq 11.38$  deg for the “thick” mode. Figures 3 and 4 show the dimensionless propulsive acceleration and the cone angle, as a function of the angle of attack, for the “thin” and “thick” modes, respectively. In both Figs. 3 and 4 there exists a non-operating zone, which is highlighted by a grey colour. In fact, for each mode, the same thrust cone angle  $\alpha$  may be obtained with two different angles of attack. For example, assuming a “thin” mode,  $\alpha = 5$  deg corresponds to either  $\phi \simeq 17.36$  deg or  $\phi \simeq 78.12$  deg. However, if  $\phi = 17.36$  deg, then  $a/[a_c (r_{\oplus}/r)^2] \simeq 0.9704$ , while  $a/[a_c (r_{\oplus}/r)^2] \simeq 0.6452$  when  $\phi = 78.12$  deg.

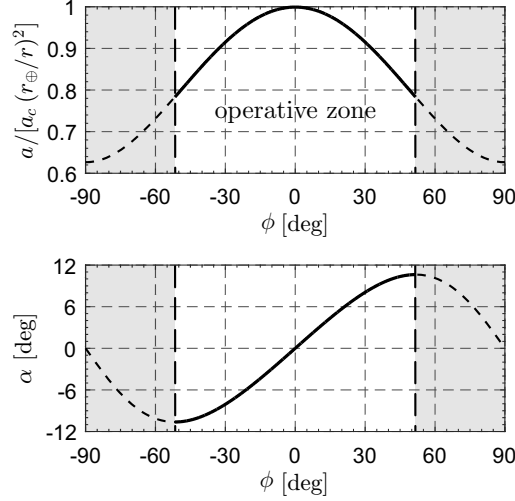


Figure 3: Dimensionless propulsive acceleration and thrust cone angle as a function of  $\phi$  (when  $\eta = 2$ ).

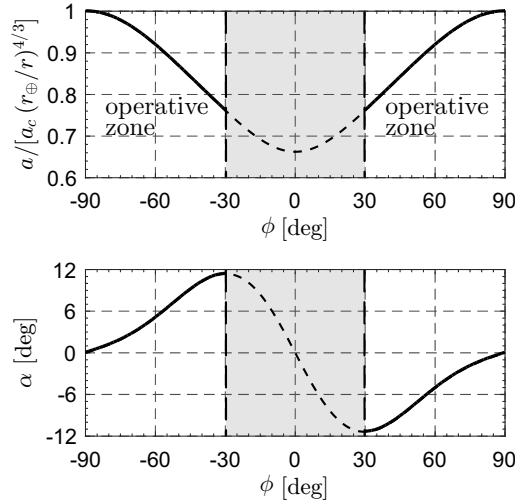


Figure 4: Dimensionless propulsive acceleration and thrust cone angle as a function of  $\phi$  (when  $\eta = 4/3$ ).

Therefore, in the rest of the paper, we will consider only intervals of  $\phi$  such that, for a given feasible  $\alpha$ , the magnitude of the propulsive acceleration is maximized. As a result, in the “thin” mode  $\phi$  ranges in the interval  $[-51.66, 51.66]$  deg, while in the “thick” mode  $\phi \in [-90, -29.77]$  deg or  $\phi \in [29.77, 90]$  deg; see Figs. 3 and 4.

### 3. Generation of displaced orbits

The thrust vector model of a Magsail-based spacecraft presented in the previous section is here used to investigate the possibility of generating and maintaining Sun-centered, circular DNKOs [15, 45]. With reference to the scheme of Fig. 5, introduce a heliocentric-ecliptic reference frame  $\mathcal{T}_\odot(O; x, y, z)$ , where  $O$  is the Sun's center of mass. Without loss of generality, the plane  $(x, y)$  coincides with the ecliptic, while

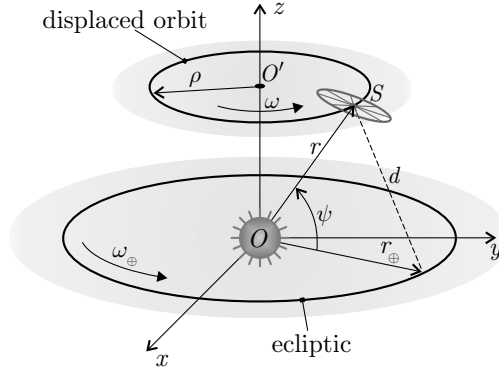


Figure 5: Conceptual scheme of a heliocentric circular DNKO. Adapted from Ref. [46].

the  $z$ -axis is parallel to the Earth's orbit angular momentum and points towards the northern celestial hemisphere [46]. A circular DNKO is a circular orbit of radius  $\rho$  and centered at  $O' \neq O$ . The displaced orbit plane is parallel to the ecliptic, and  $O'$  belongs to the  $z$ -axis. Finally, the spacecraft covers the DNKO at a given (constant) angular velocity  $\omega$ .

To fully characterize a type DNKO, it is necessary to assign three independent parameters: the elevation angle  $\psi \in [-\pi/2, \pi/2]$  rad, that is, the angle between the Sun-spacecraft vector and the ecliptic, the angular velocity  $\omega$ , and the Sun-spacecraft distance  $r$ . Note that the orbit radius  $\rho$  and the orbit displacement  $z$  may be obtained as a function of  $\psi$  and  $r$  as

$$\rho = r \cos \psi \quad (9)$$

$$z = r \sin \psi \quad (10)$$

The required thrust cone angle  $\alpha$  and characteristic acceleration  $a_c$  can be written as a function of  $\psi$ ,  $\omega$ , and  $r$ . To that end, introduce a cylindrical rotating reference frame  $\mathcal{T}_C(O; \rho, \theta, z)$  of unit vectors  $\hat{\mathbf{i}}_\rho$ ,  $\hat{\mathbf{i}}_\theta$  and  $\hat{\mathbf{i}}_z$  (see Fig. 6), defined as

$$\hat{\mathbf{i}}_\rho \triangleq \hat{\mathbf{i}}_r \cos \psi - \hat{\mathbf{i}}_z \sin \psi, \quad \hat{\mathbf{i}}_z \triangleq \hat{\mathbf{i}}_r \sin \psi + \hat{\mathbf{i}}_z \cos \psi, \quad \hat{\mathbf{i}}_\theta \triangleq \hat{\mathbf{i}}_z \times \hat{\mathbf{i}}_\rho \quad (11)$$

where  $\theta$  is the spacecraft azimuthal angle, measured from a fixed axis on the displaced orbit plane. Enforcing the balance between the propulsive, gravitational, and centrifugal accelerations, we obtain [31]

$$a \cos \alpha + \rho \omega^2 \cos \psi - \frac{\mu_\odot}{r^2} = 0 \quad (12)$$

$$a \sin \alpha - \rho \omega^2 \sin \psi = 0 \quad (13)$$

where  $\mu_\odot \simeq 1.327 \times 10^{11} \text{ km}^3/\text{s}^2$  is the Sun's gravitational parameter, while  $a$  and  $\alpha$  are obtained from Eqs. (7) and (8), respectively. After some calculations, Eqs. (12) and (13) may be rearranged to give

$$\alpha = \alpha^* \triangleq \arctan \left( \frac{(\omega/\bar{\omega})^2 \tan \psi}{1 + \tan^2 \psi - (\omega/\bar{\omega})^2} \right) \quad (14)$$

$$\frac{a_c}{\mu_\odot/r_\oplus^2} = \tilde{a}_c^* \triangleq \left( \frac{r_\oplus}{r} \right)^{2-\eta} \frac{1 - (\omega/\bar{\omega})^2 \cos^2 \psi}{C_D} \quad (15)$$



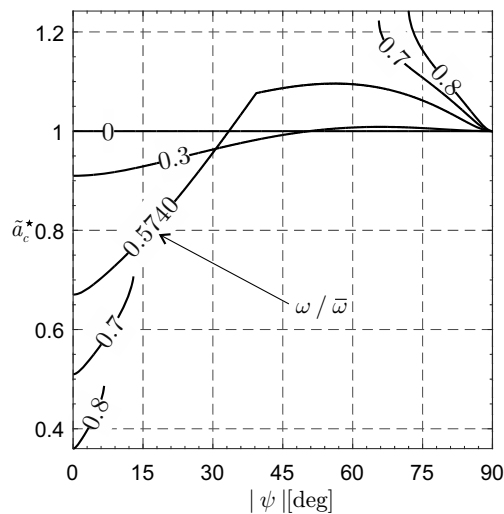


Figure 8: Required dimensionless characteristic acceleration  $\tilde{a}_c^*$  as a function of  $\psi$  and  $\omega/\bar{\omega}$  for the “thick” mode and  $r = r_\oplus$ .

The minimum value of the required characteristic acceleration is reached when  $\psi = 0$  independently of the ratio  $\omega/\bar{\omega} \in [0, 1)$ . In particular, when  $\psi = 0$ , then  $\alpha^* = 0$  and from Eq. (15).

$$\tilde{a}_c^* = \left(\frac{r_\oplus}{r}\right)^{2-\eta} \left[1 - \left(\frac{\omega}{\bar{\omega}}\right)^2\right] \quad (17)$$

When  $\omega/\bar{\omega} \geq 1$ , instead, the minimum  $\alpha^*$  is obtained for  $|\psi| = \pi/2$  rad, which implies  $\alpha^* = 0$  and  $\tilde{a}_c^* = (r_\oplus/r)^{2-\eta}$ .

### 3.1. Type I DNKO

An interesting type I DNKO [15, 32, 46] is obtained when  $\omega = \omega_\oplus \triangleq \sqrt{\mu_\odot/r_\oplus^3}$ , where  $\omega_\oplus \simeq 0.9856$  deg/day is the Earth’s mean angular velocity. Powers and Coverstone [47] called “synchronous orbits” those heliocentric circular orbits designed to match the Earth’s orbital period. In accordance with the terminology adopted in Ref. [46], these orbits will now be referred to as Earth-Synchronous Displaced Orbits (ESDOs). The condition  $\omega = \omega_\oplus$  is effective when the spacecraft mission is to observe the Earth’s polar regions [7, 8, 10, 25, 48]. In this case it is convenient to minimize the Earth-spacecraft distance  $d$  (see Fig. 5), with the constraint  $d > R_{\text{SOI}}$ , where  $R_{\text{SOI}} \simeq r_\oplus/100$  denotes the radius of the Earth’s sphere of influence. Substituting  $\omega$  with  $\omega_\oplus$ , Eqs. (14) and (15) become

$$\alpha^* = \alpha^*(\tilde{r}, \psi) = \arctan\left(\frac{\tilde{r}^3 \tan \psi}{1 + \tan^2 \psi - \tilde{r}^3}\right) \quad (18)$$

$$\tilde{a}_c^* = \tilde{a}_c^*(\tilde{r}, \psi) = \left(\frac{1 - \tilde{r}^3 \cos^2 \psi}{C_D}\right) \tilde{r}^{(\eta-2)} \quad (19)$$

while the dimensionless Earth-spacecraft distance  $\tilde{d} \triangleq d/r_\oplus$  is

$$\tilde{d} = \sqrt{\tilde{r}^2 - 2\tilde{r} \cos \psi + 1} \quad (20)$$

Figures 9–12 show the required thrust cone angle  $\alpha^*$  and the dimensionless propulsive acceleration  $\tilde{a}_c^*$  for the two magnetopause modes. In both cases, for a given  $\alpha^*$ , a smaller  $\tilde{d}$  is obtained for smaller values of  $\tilde{a}_c^*$ , while, for a given  $\tilde{a}_c^*$ ,  $\tilde{d}$  is minimized when  $\alpha^* = \pm\alpha_{\text{max}}$ . For example, consider the “thin” mode and assume that it is required to minimize  $\tilde{d}$  by using a Magsail with  $\tilde{a}_c^* = 0.05$ , that is,  $a_c \simeq 0.2965$  mm/s<sup>2</sup>. According to Fig. 10 the minimum obtainable  $\tilde{d}$  is about 0.0151, which is reached when  $\tilde{r} \simeq 0.9869$  and  $\psi \simeq 0.4336$  deg. The orbit displacement above the ecliptic is about 175 Earth’s radii.

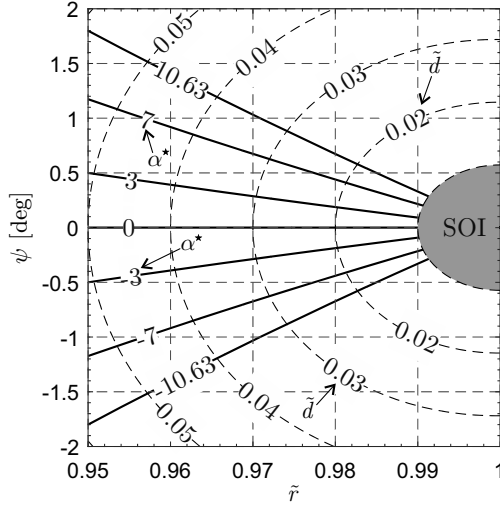


Figure 9: Required thrust cone angle  $\alpha^*$  as a function of  $\tilde{r}$  and  $\psi$  for the “thin” magnetopause mode.

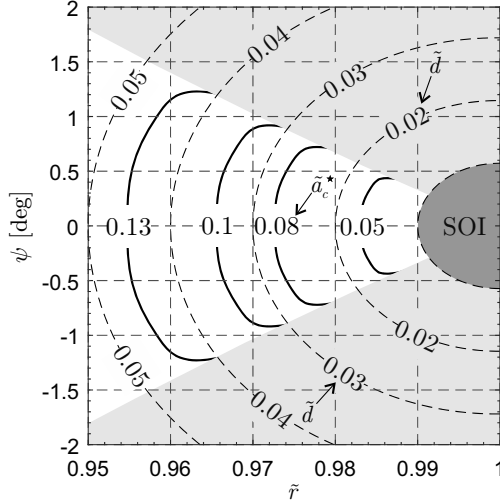


Figure 10: Required dimensionless characteristic acceleration  $\tilde{a}_c^*$  as a function of  $\tilde{r}$  and  $\psi$  for the “thin” magnetopause mode.

### 3.2. Type II DNKO

Recall that a type II DNKO has an angular velocity  $\omega$  equal to the mean motion of the circular Keplerian orbit of radius  $r$  [15, 31]. In that case  $\omega/\bar{\omega} = 1$ , and Eq. (14) reduces to [31]

$$\alpha^* = \arctan(\cot \psi) \quad (21)$$

which means that  $\psi$  and  $\alpha^*$  are complementary angles, that is,  $|\psi + \alpha^*| = \pi/2$  rad. Therefore, type II DNKOs can be maintained with a Magsail only if  $|\psi| \geq \alpha_{\max}$ . The required characteristic acceleration becomes

$$\tilde{a}_c^* = \frac{\sin^2 \psi}{C_D} \tilde{r}^{(\eta-2)} \quad (22)$$

where  $\tilde{r} \triangleq r/r_{\oplus}$ . In a “thin” mode,  $\tilde{a}_c^* = (\sin \psi)^2/C_D$ , and the required propulsive acceleration is independent of the Sun-spacecraft distance  $r$ , as is shown in Fig. 13. Figure 14 illustrates the variation of  $\tilde{a}_c^*$  as a function of  $\psi$  and  $\tilde{r}$  for the “thick” magnetopause mode. Note that, when  $|\psi| = \pi/2$  rad, the spacecraft is in a heliostationary condition, that is, the thrust exactly balances the local gravitational pull.

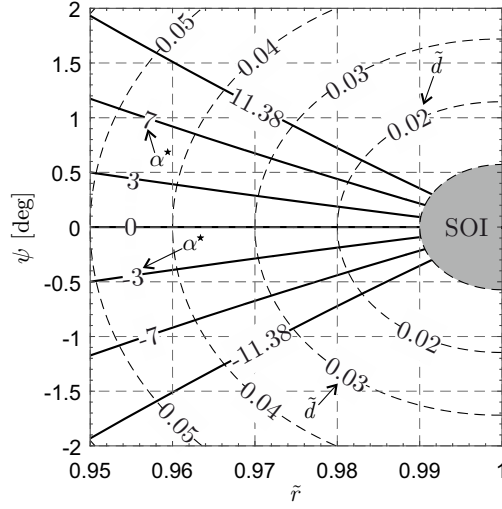


Figure 11: Required thrust cone angle  $\alpha^*$  as a function of  $\tilde{r}$  and  $\psi$  for the “thick” magnetopause mode.

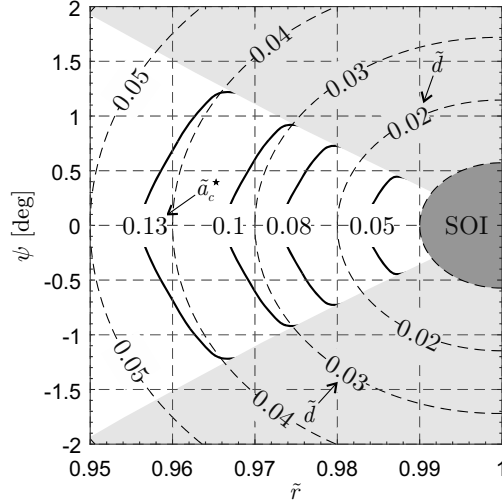


Figure 12: Required dimensionless characteristic acceleration  $\tilde{a}_c^*$  as a function of  $\tilde{r}$  and  $\psi$  for the “thick” magnetopause mode.

To summarize, Eqs. (14) and (15) quantify the performance required to generate a circular DNKO. It is now advisable to verify whether a Magsail is able to maintain a given DNKO in a passive way, or an active control system is necessary. This aspect is addressed in the next section by analyzing the stability of its linearized dynamics.

#### 4. Linear stability analysis

An important point is the stability analysis of DNKOs, which is here addressed by looking for the conditions that ensure a (linearly) stable motion. Paralleling the procedure described in Ref. [31], consider

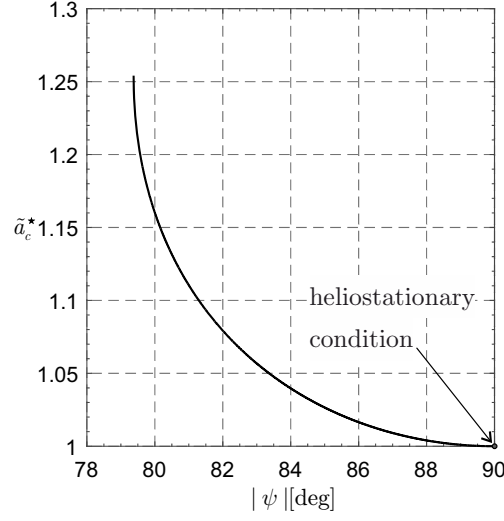


Figure 13: Required performance for the maintenance of a type II DNKO with a “thin” mode Magsail.

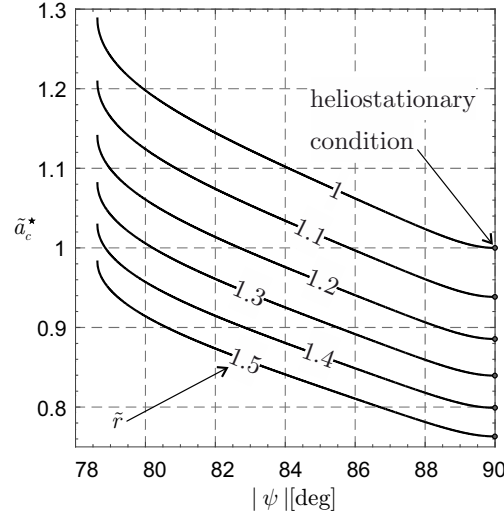


Figure 14: Required performance for the maintenance of a type II DNKO with a “thick” mode Magsail.

the spacecraft equations of motion in the cylindrical rotating reference frame  $\mathcal{T}_C(O; \rho, \theta, z)$

$$\ddot{\rho} = -\frac{\mu_{\odot}}{r^3} \rho + \rho \dot{\theta}^2 + a \cos(\alpha + \psi) \quad (23)$$

$$\ddot{\theta} = -\frac{2\dot{\rho}\dot{\theta}}{\rho} \quad (24)$$

$$\ddot{z} = -\frac{\mu_{\odot}}{r^3} z + a \sin(\alpha + \psi) \quad (25)$$

The perturbative dynamics is obtained by introducing an error in the spacecraft initial position, which models an error in the orbital insertion. To that end, the initial orbit radius and displacement may be

written as

$$\rho(t_0) \triangleq \rho_0 + \delta_\rho(t_0) \quad (26)$$

$$z(t_0) \triangleq z_0 + \delta_z(t_0) \quad (27)$$

where the subscript 0 denotes the nominal value (being  $t_0 \triangleq 0$  the initial time), while  $\delta_\rho(t) \ll \rho_0$  and  $\delta_z(t) \ll z_0$  are the errors in the orbit radius and displacement, respectively. It is also assumed that no error exists in the initial velocity (i.e.,  $\rho(t_0)\dot{\theta}(t_0) = \rho_0\omega_0$ ), while  $\alpha(t) = \alpha_0$  at any time  $t$ . Note that, from Eq. (24), it follows that  $\rho^2\dot{\theta}$  is constant and, in particular

$$\rho^2\dot{\theta} \simeq \rho_0^2\omega_0 \left[ 1 + \frac{\delta_\rho(t_0)}{\rho_0} \right] \quad (28)$$

Using the latter transformation, and recalling Eq. (28), the linearized expressions of  $r^\lambda$  (with  $\lambda \in \mathbb{R}$ ),  $a$ ,  $\rho\dot{\theta}^2$ ,  $\cos\psi$ , and  $\sin\psi$  become

$$r^\lambda \simeq r_0^\lambda \left( 1 + \lambda \cos\psi_0 \frac{\delta_\rho}{r_0} + \lambda \sin\psi_0 \frac{\delta_z}{r_0} \right) \quad (29)$$

$$a \simeq \frac{\mu_\odot}{r_0^2} \frac{f}{\cos\alpha_0} \left( 1 - \eta \cos\psi_0 \frac{\delta_\rho}{r_0} - \eta \sin\psi_0 \frac{\delta_z}{r_0} \right) \quad (30)$$

$$\rho\dot{\theta}^2 \simeq \rho_0\omega_0^2 \left[ 1 - 3 \frac{\delta_\rho}{\rho_0} + 2 \frac{\delta_\rho(t_0)}{\rho_0} \right] \quad (31)$$

$$\cos\psi \simeq \cos\psi_0 \left( 1 - \cos\psi_0 \frac{\delta_\rho}{r_0} - \sin\psi_0 \frac{\delta_z}{r_0} + \frac{\delta_\rho}{\rho_0} \right) \quad (32)$$

$$\sin\psi \simeq \sin\psi_0 \left( 1 - \cos\psi_0 \frac{\delta_\rho}{r_0} - \sin\psi_0 \frac{\delta_z}{r_0} + \frac{\delta_z}{z_0} \right) \quad (33)$$

where

$$f \triangleq 1 - \left( \frac{\omega_0}{\bar{\omega}} \right)^2 \cos^2\psi_0 \quad (34)$$

The perturbation equations are obtained from Eqs. (23) and (25) by subtracting the corresponding equilibrium equation, that is

$$-1 + f(1 - \tan\alpha_0 \tan\psi_0) + \left( \frac{\omega_0}{\bar{\omega}} \right)^2 = 0 \quad (35)$$

$$-1 + f(1 + \tan\alpha_0 \cot\psi_0) = 0 \quad (36)$$

where  $\bar{\omega} \triangleq \sqrt{\mu_\odot/r_0^3}$ . As a result, the perturbative equations can be written in compact form as

$$\delta_\rho'' = a_{11}\delta_\rho + a_{12}\delta_z + 2\delta_\rho(t_0) \quad (37)$$

$$\delta_z'' = a_{21}\delta_\rho + a_{22}\delta_z \quad (38)$$

where the prime symbol denotes a derivative with respect to the dimensionless time  $\tilde{t} \triangleq \bar{\omega}t$ , while the coefficients  $a_{ij}$  are given by

$$a_{11} = 3\cos^2\psi_0 - 1 + f[\sin^2\psi_0 - \eta\cos^2\psi_0 + (1+\eta)\tan\alpha_0\sin\psi_0\cos\psi_0] - 3\left(\frac{\omega_0}{\bar{\omega}}\right)^2 \quad (39)$$

$$a_{12} = 3\sin\psi_0\cos\psi_0 - f[(1+\eta)\sin\psi_0\cos\psi_0 + \tan\alpha_0(\cos^2\psi_0 - \eta\sin^2\psi_0)] \quad (40)$$

$$a_{21} = 3\sin\psi_0\cos\psi_0 - f[(1+\eta)\sin\psi_0\cos\psi_0 - \tan\alpha_0(\sin^2\psi_0 - \eta\cos^2\psi_0)] \quad (41)$$

$$a_{22} = 3\sin^2\psi_0 - 1 + f[\cos^2\psi_0 - \eta\sin^2\psi_0 - (1+\eta)\tan\alpha_0\sin\psi_0\cos\psi_0] \quad (42)$$

with

$$\tan \alpha_0 \triangleq \frac{(\omega_0/\bar{\omega})^2 \tan \psi_0}{1 + \tan^2 \psi_0 - (\omega_0/\bar{\omega})^2} \quad (43)$$

The poles of the linearized system are the roots of the associated characteristic polynomial, that is

$$s^4 + b s^2 + c = 0 \quad (44)$$

where

$$b \triangleq -(a_{11} + a_{22}) \quad (45)$$

$$c \triangleq a_{11} a_{22} - a_{12} a_{21} \quad (46)$$

Because Eq. (44) is a biquadratic equation, the (marginal) stability of the linearized system requires the roots of the characteristic equation (44) to be purely imaginary. The condition to be met is therefore  $b > 2\sqrt{c}$ , which is satisfied for both Magsail modes as long as  $c > 0$ . For both magnetopause modes, the regions for which  $a_c < 0$  or  $\alpha > \alpha_{\max}$  are infeasible; see Figs. 15 and 16. Also, as far as the “thin” mode is concerned, the feasible regions are always linearly stable because  $c > 0$ , as is illustrated in Fig. 17. When

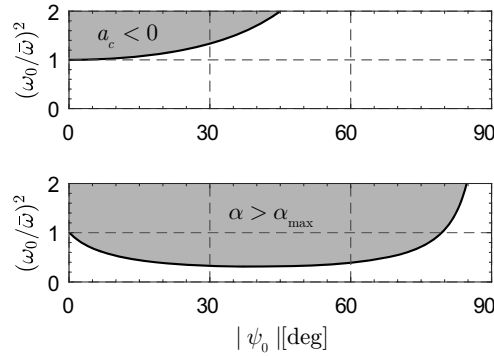


Figure 15: Constraints for the feasibility and linear stability of DNKOs with  $\eta = 2$ .

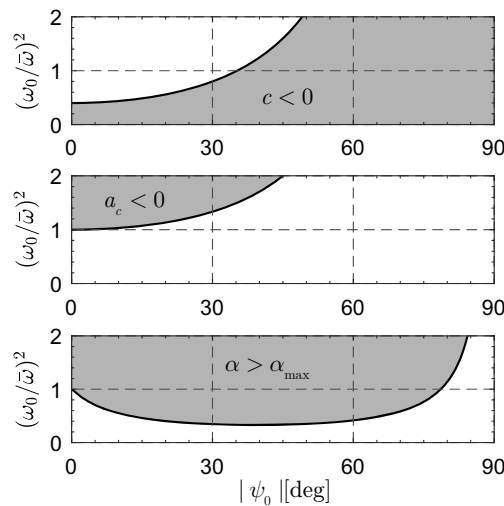


Figure 16: Constraints on feasibility and linear stability of DNKOs with  $\eta = 4/3$ .

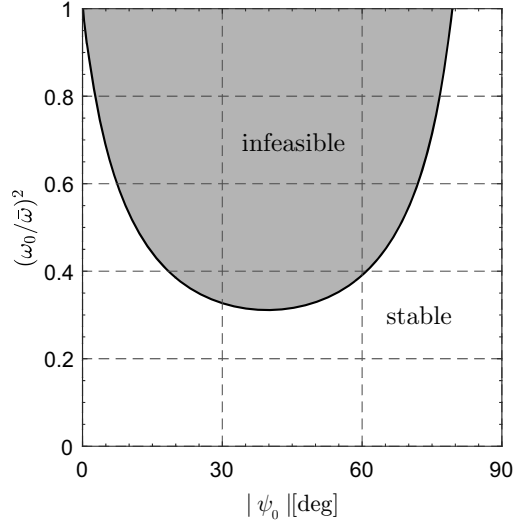


Figure 17: Stable and infeasible regions of the linearized dynamics for  $\eta = 2$ .

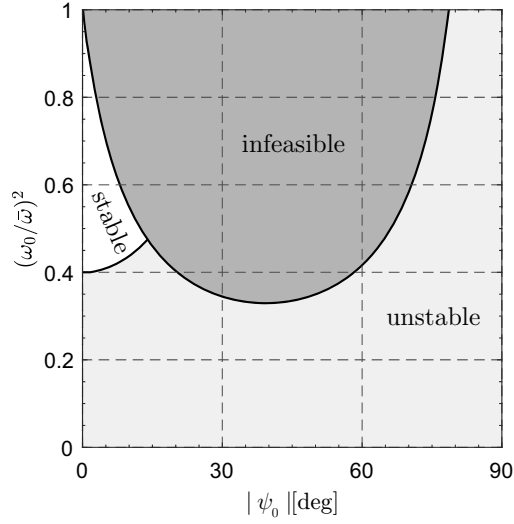


Figure 18: Stable, unstable and infeasible regions of the linearized dynamics when  $\eta = 4/3$ .

$\eta = 4/3$ , instead, Fig. 16 shows that the coefficient  $c$  may be either positive or negative and, as such, stable, unstable and infeasible regions are possible; see Fig. 18. Invoking the Lyapunov's linearization method [49], the instability of the linearized dynamics implies the instability of the nonlinear system. Conversely, the marginal stability of the linearized dynamics is only a necessary (but not sufficient) condition for the stability of the nonlinear system. A number of numerical simulations has been conducted to verify the stability of the nonlinear dynamics, showing that the stability regions are slightly narrower than those reported in Figs. 17 and 18.

#### 4.1. Mission application

Consider the problem of maintaining an ESDO, that is, a circular, displaced, non-Keplerian orbit that the spacecraft covers following the Earth during its revolution around the Sun ( $\omega = \omega_{\oplus}$ ). In particular, the exemplary mission is to place the spacecraft in a convenient position relative to the Earth in order to continuously observe its high-latitude regions. This case is similar to the pole-sitter mission concept

described by Ceriotti et al. [8], in which a solar electric thruster or a hybrid propulsion system (i.e., a combination of solar sail and solar electric thruster) is used to maintain an Earth-spacecraft distance of about 0.018 au. Such a value is chosen to ensure a correct spatial resolution to the scientific instruments. Assume  $\tilde{d} = \tilde{d}_0 = 0.018$  and consider a Magsail with a “thick” magnetopause mode (i.e.,  $\eta = 4/3$ ). From Eq. (20) it is possible to find all the possible combinations of  $\tilde{r}$  and  $\psi$  such that  $\tilde{d} = 0.018$ ; see Fig. (19).

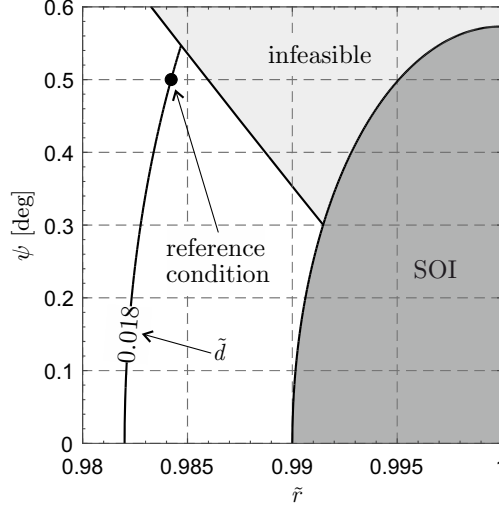


Figure 19: Reference condition for the case study ( $\eta = 4/3$ ).

Because a higher elevation angle allows a better coverage of the Earth’s polar zones to be obtained, a reference condition is chosen such that  $\tilde{r} = \tilde{r}_0 \simeq 0.9842$  and  $\tilde{\psi} = \psi_0 = 0.5$  deg; see Fig. (19). From Eqs. (18) and (19) the required thrust cone angle and characteristic acceleration may be calculated as a function of  $\tilde{r}_0$  and  $\psi_0$ , and the result is  $\tilde{a}_c^* \simeq 0.0712$  (that is,  $a_c \simeq 0.42$  mm/s<sup>2</sup>) and  $\tilde{\alpha}^* \simeq 10.11$  deg.

In this case  $(\omega_0/\bar{\omega})^2 = (\omega_{\oplus}/\bar{\omega})^2 \simeq 0.9534$  and, therefore, the linearized system is stable; see Fig. 18. The stability of the complete dynamics is also checked by numerical simulation, in which Eqs. (23)–(25) are integrated in double precision using a variable order Adams-Bashforth-Moulton solver scheme with absolute and relative errors of  $10^{-12}$  and a time span of 50 years. The error in the orbit insertion is modeled assuming  $\delta_\rho(t_0) = \delta_z(t_0) = 0.001$ , which corresponds to a distance error of about  $2 \times 10^5$  km; see Eqs. (26) and (27). The simulation results involving the normalized distance ( $r/r_0$ ) and elevation angle ( $\psi/\psi_0$ ) are reported in Fig. 20. Note that the fluctuations with respect to the reference values are less than 0.4% and 8% for  $r$  and  $\psi$ , respectively.

Finally consider the radial ( $v_r$ ), azimuthal ( $v_\theta$ ) and normal ( $v_\psi$ ) components of the spacecraft velocity, defined as

$$v_r \triangleq \dot{\rho} \cos \psi + \dot{z} \sin \psi \quad (47)$$

$$v_\theta \triangleq \rho \dot{\theta} \quad (48)$$

$$v_\psi \triangleq \dot{z} \cos \psi - \dot{\rho} \sin \psi \quad (49)$$

In the reference condition  $v_{r_0} = v_{\psi_0} = 0$ , and  $v_{\theta_0} = \rho_0 \omega_{\oplus} \simeq 29.3$  km/s. The time variation of the velocity components are reported, in a dimensionless form, in Fig. 21. Note that the fluctuations of  $\{v_r, v_\theta, v_\psi\}$  are very small, less than 0.02% of  $v_{\theta_0}$  (about 59 m/s).

## 5. Conclusions

This paper has analyzed the problem of generating circular, displaced, non-Keplerian orbits around the Sun using a Magsail-based spacecraft. Starting from a recent mathematical model for the description

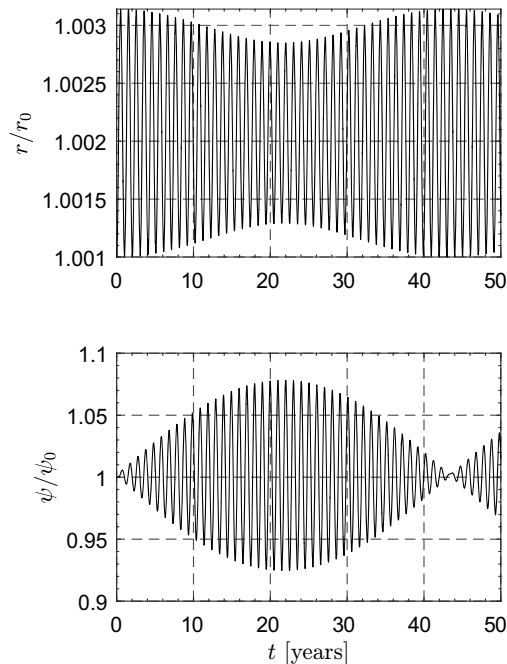


Figure 20: Long-time variation of the spacecraft perturbed states for the case study.

of the Magsail propulsive acceleration vector, the requirements necessary to guarantee a displaced orbit maintenance have been expressed in terms of characteristic acceleration and thrust cone angle. Due to the small value of the maximum obtainable thrust cone angle, some combinations of angular velocity and elevation angle are unfeasible, while others, albeit feasible, turn out to be unstable at linear order. In particular, unstable and marginally stable regions have been investigated by assuming a position error in the orbital insertion.

A natural extension of this work is to investigate a suitable control system that is able to reduce or even delete the unstable regions. This result may be accomplished, for example, by modulating the electrical current flowing in the ring, or by reorienting the thrust vector. Another interesting application of the Magsail concept is represented by the achievement of heliocentric elliptic displaced non-Keplerian orbits. In this last case, however, the necessary control system is more involved, since it must be able to vary the propulsive acceleration magnitude and, at the same time, the thrust vector direction.

## References

- [1] S. Gong, J. Li, F. Jiang, Interplanetary trajectory design for a hybrid propulsion system, *Aerospace Science and Technology* 45 (2015) 104–113, doi: 10.1016/j.ast.2015.04.020.
- [2] H. Shang, S. Wang, W. Wu, Design and optimization of low-thrust orbital phasing maneuver, *Aerospace Science and Technology* 42 (2015) 365–375, doi: 10.1016/j.ast.2015.02.003.
- [3] J. Mu, S. Gong, J. Li, Reflectivity-controlled solar sail formation flying for magnetosphere mission, *Aerospace Science and Technology* 30 (1) (2013) 339–348, doi: 10.1016/j.ast.2013.09.002.
- [4] S. Firuzi, S. Gong, Refractive sail and its applications in solar sailing, *Aerospace Science and Technology* 77 (2018) 362–372, doi: 10.1016/j.ast.2018.03.016.
- [5] P. Anderson, M. Macdonald, Extension of highly elliptical earth orbits using continuous low-thrust propulsion, *Journal of Guidance, Control, and Dynamics* 36 (1) (2013) 282–292, doi: 10.2514/1.55304.
- [6] R. J. McKay, M. MacDonal, J. Biggs, C. McInnes, Survey of highly-non-Keplerian orbits with low-thrust propulsion, *Journal of Guidance, Control, and Dynamics* 34 (3) (2011) 645–666, doi: 10.2514/1.52133.
- [7] M. Ceriotti, C. R. McInnes, Systems design of a hybrid sail pole-sitter, *Advances in Space Research* 48 (11) (2011) 1754–1762, doi: 10.1016/j.asr.2011.02.010.
- [8] M. Ceriotti, J. Heiligers, C. R. McInnes, Trajectory and spacecraft design for a pole-sitter mission, *Journal of Spacecraft and Rockets* 51 (1) (2014) 311–326, doi: 10.2514/1.A32477.

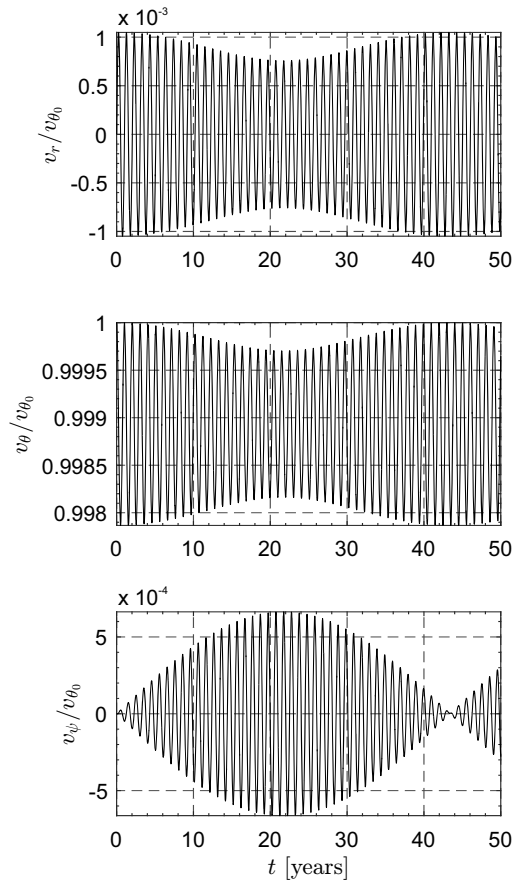


Figure 21: Long-time variation of the spacecraft velocity components for the case study.

- [9] M. MacDonald, R. J. McKay, M. Vasile, F. B. De Frescheville, J. Biggs, C. R. McInnes, Low-thrust-enabled highly-non-Keplerian orbits in support of future Mars exploration, *Journal of Guidance, Control, and Dynamics* 34 (5) (2011) 1396–1411, doi: 10.2514/1.52602.
- [10] J. Heiligers, M. Ceriotti, C. R. McInnes, Displaced geostationary orbit design using hybrid sail propulsion, *Journal of Guidance, Control, and Dynamics* 34 (6) (2011) 1852–1866, doi: 10.2514/1.53807.
- [11] Y. Liu, J. Heiligers, M. Ceriotti, Loosely-displaced geostationary orbits with hybrid sail propulsion, *Aerospace Science and Technology* 79 (2018) 105–117, doi: 10.1016/j.ast.2018.05.034.
- [12] C. R. McInnes, Displaced non-Keplerian orbits using impulsive thrust, *Celestial Mechanics and Dynamical Astronomy* 110 (3) (2011) 199–215, doi: 10.1007/s10569-011-9351-5.
- [13] A. Caruso, A. A. Quarta, G. Mengali, Elliptic displaced orbit approximation with equally spaced impulses, *Journal of Guidance, Control, and Dynamics* 42 (2) (2019) 411–415, doi: 10.2514/1.G003900.
- [14] C. R. McInnes, Dynamics, stability, and control of displaced non-Keplerian orbits, *Journal of Guidance, Control, and Dynamics* 21 (5) (1998) 799–805, doi: 10.2514/2.4309.
- [15] C. R. McInnes, *Solar Sailing: Technology, Dynamics and Mission Applications*, Springer-Praxis Series in Space Science and Technology, Springer-Verlag, 2004.
- [16] P. Janhunen, Electric sail for spacecraft propulsion, *Journal of Propulsion and Power* 20 (4) (2004) 763–764, doi: 10.2514/1.8580.
- [17] P. Janhunen, A. Sandroos, Simulation study of solar wind push on a charged wire: basis of solar wind electric sail propulsion, *Annales Geophysicae* 25 (3) (2007) 755–767, doi: 10.5194/angeo-25-755-2007.
- [18] G. Mengali, A. A. Quarta, P. Janhunen, Electric sail performance analysis, *Journal of Spacecraft and Rockets* 45 (1) (2008) 122–129, doi: 10.2514/1.31769.
- [19] D. G. Andrews, R. M. Zubrin, Use of magnetic sails for Mars exploration missions, in: *AIAA/ASME/SAE/ASEE 25th Joint Propulsion Conference*, no. AIAA 89-2861, Monterey, CA, 1989.
- [20] D. G. Andrews, R. M. Zubrin, Progress in magnetic sails, in: *AIAA/ASME/SAE/ASEE 26th Joint Propulsion Conference*,

- no. AIAA 90-2367, Orlando, FL, 1990.
- [21] D. G. Andrews, R. M. Zubrin, Magnetic sails and interstellar travel, *Journal of the British Interplanetary Society* 43 (6) (1990) 265–272 .
- [22] R. M. Zubrin, D. G. Andrews, Magnetic sails and interplanetary travel, *Journal of Spacecraft and Rockets* 28 (2) (1991) 197–203, doi: 10.2514/3.26230.
- [23] R. M. Zubrin, The use of magnetic sails to escape from low earth orbit, *Journal of the British Interplanetary Society* 46 (3) (1992) 3–10, doi: 10.2514/6.1991-3352.
- [24] J. Bookless, C. R. McInnes, Dynamics and control of displaced periodic orbits using solar-sail propulsion, *Journal of Guidance, Control, and Dynamics* 29 (3) (2006) 527–537, doi: 10.2514/1.15655.
- [25] S. Gong, J. Li, Spin-stabilized solar sail for displaced solar orbits, *Aerospace Science and Technology* 32 (1) (2014) 188–199, doi: 10.1016/j.ast.2013.10.002.
- [26] S. Gong, H. Baoyin, J. Li, Relative orbit design and control of formation around displaced solar orbits, *Aerospace Science and Technology* 12 (2) (2008) 195–201, doi: 10.1016/j.ast.2007.05.004.
- [27] M. Song, X. He, D. He, Displaced orbits for solar sail equipped with reflectance control devices in Hill’s restricted three-body problem with oblateness, *Astrophysics and Space Science* 361 (10), doi: 10.1007/s10509-016-2915-9.
- [28] M. Xu, S. Xu, Nonlinear dynamical analysis for displaced orbits above a planet, *Celestial Mechanics and Dynamical Astronomy* 102 (4) (2008) 327–353, doi: 10.1007/s10569-008-9171-4.
- [29] X. Pan, M. Xu, H. Huang, X. Pei, Y. Dong, Nonlinear dynamics of displaced non-keplerian orbits with low-thrust propulsion, *Communications in Nonlinear Science and Numerical Simulation* 66 (2019) 61–83, doi: 10.1016/j.cnsns.2018.06.005.
- [30] W. Wang, G. Mengali, A. Quarta, J. Yuan, Analysis of relative motion in non-Keplerian orbits via modified equinoctial elements, *Aerospace Science and Technology* 58 (2016) 389–400, doi: 10.1016/j.ast.2016.09.001.
- [31] L. Niccolai, A. A. Quarta, G. Mengali, Electric sail-based displaced orbits with a refined thrust model, *Proceedings of the Institution of Mechanical Engineers, Part G: Journal of Aerospace Engineering* 232 (3) (2018) 423–432, doi: 10.1177/0954410016679195.
- [32] L. Niccolai, A. A. Quarta, G. Mengali, Electric sail elliptic displaced orbits with advanced thrust model, *Acta Astronautica* 138 (2017) 503–511, doi: 10.1016/j.actaastro.2016.10.036.
- [33] K. Fujita, Particle simulation of moderately-sized magnetic sails, *The Journal of Space Technology and Science* 20 (2) (2004) 26–31 .
- [34] H. Nishida, H. Ogawa, I. Funaki, K. Fujita, H. Yamakawa, Y. Nakayama, Two-dimensional magnetohydrodynamic simulation of a magnetic sail, *Journal of Spacecraft and Rockets* 43 (3) (2006) 667–672, doi: 10.2514/1.15717.
- [35] I. Funaki, H. Kojima, H. Yamakawa, Y. Nakayama, Y. Shimizu, Laboratory experiment of plasma flow around magnetic sail, *Astrophysics and Space Science* 307 (1–3) (2007) 63–68, doi: 10.1007/s10509-006-9251-4.
- [36] K. Ueno, I. Funaki, T. Kimura, H. Horisawa, H. Yamakawa, Thrust measurement of a pure magnetic sail using parallelogram-pendulum method, *Journal of Propulsion and Power* 25 (2) (2009) 536–539, doi: 10.2514/1.39211.
- [37] Y. Kajimura, H. Usui, I. Funaki, K. Ueno, M. Nunami, I. Shinohara, M. Nakamura, H. Yamakawa, Hybrid particle-in-cell simulations of magnetic sail in laboratory experiment, *Journal of Propulsion and Power* 26 (1) (2010) 159–166, doi: 10.2514/1.45096.
- [38] Y. Ashida, I. Funaki, H. Yamakawa, Y. Kajimura, H. Kojima, Thrust evaluation of a magnetic sail by flux-tube model, *Journal of Propulsion and Power* 28 (3) (2012) 642–651, doi: 10.2514/1.B34332.
- [39] Y. Kajimura, I. Funaki, M. Matsumoto, I. Shinohara, H. Usui, H. Yamakawa, Thrust and attitude evaluation of magnetic sail by three-dimensional hybrid particle-in-cell code, *Journal of Propulsion and Power* 28 (3) (2012) 652–663, doi: 10.2514/1.B34334.
- [40] H. Nishida, I. Funaki, Analysis of thrust characteristics of a magnetic sail in a magnetized solar wind, *Journal of Propulsion and Power* 28 (3) (2012) 636–641, doi: 10.2514/1.B34260.
- [41] H. Kojima, I. Funaki, Y. Shimizu, H. Yamakawa, S. Shinohara, Y. Nakayama, Experimental simulation of a plasma flow around magnetic sail, in: 29th International Electric Propulsion Conference, no. IEPC-2005-107, Princeton, NJ, 2005.
- [42] Y. Murayama, K. Ueno, Y. Oshio, H. Horisawa, I. Funaki, Preliminary results of magnetic field measurements on multi-coil magnetic sail in laboratory experiment, *Vacuum* (2018) in press, doi: 10.1016/j.vacuum.2018.05.004.
- [43] A. A. Quarta, G. Mengali, G. Aliasi, Optimal control laws for heliocentric transfers with a magnetic sail, *Acta Astronautica* 89 (2013) 216–225, doi: 10.1016/j.actaastro.2013.04.018.
- [44] M. Huo, G. Mengali, A. A. Quarta, Electric sail thrust model from a geometrical perspective, *Journal of Guidance, Control, and Dynamics* 41 (3) (2018) 734–740, doi: 10.2514/1.G003169.
- [45] G. Mengali, A. A. Quarta, Non-Keplerian orbits for electric sails, *Celestial Mechanics and Dynamical Astronomy* 105 (1) (2009) 179–195, doi: 10.1007/s10569-009-9200-y.
- [46] A. A. Quarta, G. Mengali, M. Bassetto, Optimal solar sail transfers to circular Earth-synchronous displaced orbits, *In press. Astrodynamics* .
- [47] R. B. Powers, V. L. Coverstone, Optimal solar sail orbit transfers to synchronous orbits, *Journal of the Astronautical Sciences* 49 (2) (2001) 269–281 .
- [48] M. Ceriotti, C. R. McInnes, B. L. Diedrich, The pole-sitter mission concept: an overview of recent developments and possible future applications, in: 62nd International Astronautical Congress 2011, IAC 2011, Vol. 3, Cape Town, South Africa, 2011, pp. 2543–2559.
- [49] J. E. Slotine, W. Li, *Applied Nonlinear Control*, Prentice-Hall, Englewood Cliffs, NJ, 1991, Ch. 3, pp. 53–57.